Scientia Iranica F (2014) 21(6), 2468–2478

Sharif University of Technology
Scientia Iranica
Transactions F: Nanotechnology
www.scientiairanica.com

Solvothermal synthesis of $CuMS_2$ (M=Al, In, Fe) nanoparticles and effect of coordinating solvent on the crystalline structure

Y. Vahidshad[a,b], R. Ghasemzadeh[a,*], A. Iraji Zad[c], S.M. Mirkazemi[a] and A. Masoud[b]

a. *School of Metallurgy and Material Engineering, Iran University of Science and Technology, Tehran, P.O. Box 16844, Iran.*
b. *Department of Material Research, Engineering Research Institute, Tehran, P.O. Box 1344575-411, Iran.*
c. *Department of Physics, Sharif University of Technology, Tehran, P.O. Box 11155-9161, Iran.*

Received 19 February 2014; received in revised form 14 October 2014; accepted 17 November 2014

KEYWORDS
Chalcopyrite;
Wurtzite;
Structural properties;
Optical properties;
Solvothermal.

Abstract. $CuMS_2$ (M=Al, In, Fe) ternary compounds were synthesized via the facile polyol method in autoclave. Depending on the functional groups of solvent and surfactant, the structure of the nanocrystals can be controlled in the form of wurtzite or chalcopyrite. The chalcopyrite structure was obtained when the precursors solved in the mixture of diethylene glycol, polyethylene glycol 600 and ammonium hydroxide. When the solvent was replaced by ethylene diamine, the wurtzite was obtained along with chalcopyrite (polytypism). The products were characterized by X-Ray Diffraction (XRD) for analysis of structural properties, Transmission Electron Microscopy (TEM) for studying morphological properties, and absorbance spectrophotometer (UV-Vis-NIR) and photoluminescence (PL) for analysis of optical properties. The different optical band gap for $CuAlS_2$ (3.48 eV), $CuInS_2$ (1.51 eV) and $CuFeS_2$ (0.65 eV) could be utilized for absorbance material in a whole range of sunlight wavelengths. The possible formation mechanism was also discussed.

1. Introduction

I-III-VI_2 ternary compounds are known as important semiconductors that can be utilized as in photovoltaic, optic, electronic and bioimaging applications. The $CuMS_2$ ternary compounds (M=Al, Ga, In and Fe), due to a high absorption coefficient ($> 10^5$ cm^{-1}), changeable electrical conductivity (p-type or n-type) and tunable band gap (0.6-3.5 eV), can be ideally utilized in thin film solar cells as absorbance materials in all the wavelength ranges of sunlight [1-5]. There are two general approaches to producing these ternary compounds. Using H_2S gas to pass through the production of intermetallic compounds (in a vacuum chamber) is the first method. The wet chemical method (non-vacuum) to produce ternary $CuMS_2$ compounds is the second. Low time-consumption, low cost, and low material waste, besides well-controlled stoichiometry, are advantages of the wet chemical process [6-12]. Among wet chemical synthesis, the solvothermal process is one of the best wet chemical methods, because the control of stoichiometry is simple for the synthesis of nanocrystals (NCs) along with good crystalline quality, without any post heat treatment [13-19]. This method proposes the use of temperatures well above their boiling solvent to produce high pressure, which can be helpful to easily dissolve and complete the formation of chemical compounds with the solvent in the presence of a capping agent (polyethylene glycol, oleic acid, etc.) [20-21]. Sulfide chalcogenides compounds, such

*. *Corresponding author. Tel.: +98 21 7724540; Fax: +98 21 77240480*
E-mail address: rgzadeh@iust.ac.ir (R. Ghasemzadeh)

as $CuIn_xGa_{1-x}S_2$, $CuInS_2$, $CuAlS_2$ and $CuFeS_2$, are more environmentally friendly than selenium compounds. Currently, monodisperse nanoparticles with small particle size and narrow distribution, with regard to low cost techniques for the synthesis of non-toxic $CuMS_2$ compounds, play a key role in photovoltaic or light emitting diode industries [22-34]. In our previous work, we studied the various conditions of synthesis for $CuAlS_2$ and $CuInS_2$ [25-27]. The aim of this study is to understand the ternary compound formation for the alloying of these compounds in the future. Therefore, it is important to investigate the common rules or mechanisms behind this process, which contribute to the controllable synthesis of these compounds. In this research, we use the solvothermal reaction in an autoclave for synthesis of $CuMS_2$ ternary compounds, where M is Al, In and Fe. The effect of different functional groups on the structural and optical properties of $CuAlS_2$, $CuInS_2$ and $CuFeS_2$ is investigated.

2. Experimental

All used chemicals were analytical grade: Copper chloride (for analysis EMSURE®ACS, Merck), aluminum trichloride (anhydrous powder sublimed for synthesis, Merck), indium sulfate (anhydrous for synthesis, Merck), iron trichloride (for analysis EMSURE®ACS, Merck), and thiourea (GR for analysis ACS, Merck); diethylene glycol ($(CH_2CH_2OH)_2O$), polyethylene glycol 600 ($HO(C_2H_4O)_nH$) and ammonium hydroxide (NH_4OH) were used as initial materials provided by the Merck company. The $CuAlS_2$, $CuInS_2$ and $CuFeS_2$ NCs were synthesized by a solvothermal approach in an autoclave. First, stoichiometric amounts of metal salts ($AlCl_3$ or $InCl_3$ or $FeCl_3$ and CuCl) were dissolved into 10 cc PEG and 30 cc DEG. Then, the solution was heated under argon until 140°C in a three neck flask and stirred for at least 60 min to obtain a dark blue solution. In another vessel, the 40 mmol thiourea ($SC(NH_2)_2$) and amount of reducing agent were dissolved into 10 cc DEG at 30°C and stirred for at least 60 min to obtain a transparent solution. Subsequently, the second solution was injected into the first solution (including metal cations) at the defined temperatures (140°C) and stirred for 15 min. The solution in the flask quickly turned black. Then, the solution was moved into the autoclave and sealed. After that, the temperature rose to 210-220°C for a specified time, and the crystallinity was quite good. After processing completion, the autoclave was cooled down to room temperature, the products were centrifuged, washed several times with distilled water and ethanol and, finally, dried at 60°C for 10 h under air condition (see Table 1 for details concerning solution preparation). As can be seen, the sample codes that were used in this study were in the CIAFS-WA-n format. The C, I, A, F and S symbols indicate Cu, In, Al, Fe and S elements, while the W and A symbol showed the "with autoclave" synthesis, and n indicated the

Table 1. Experimental detail of polyol synthesis method.

Sample no.	NH_2/(OH_{DEG} + OH_{PEG})	EDA [a]	DEG [b]	PEG [c]	(Cu:In: Al:Fe)	Cation temp.	Plane	Intensity	Structure
CAS-WA-14	0.45/0.1620	30 cc	15 cc	15 cc	(1:0:1:0)	70°C	(112)	671	CH [d]-$CuAlS_2$
CAS-WA-19	0/0.5815	0 cc	55 cc	10 cc	(1:0:1:0)	140°C	(112)	1200	CH-$CuAlS_2$
CFS-WA-2	0.45/0.1620	30 cc	15 cc	15 cc	(1:0:0:1)	70°C	(112)	424	(W [e]+CH)-$CuFeS_2$
CFS-WA-3	0/0.5815	0 cc	55 cc	10 cc	(1:0:0:1)	140°C	(112)	1218	CH-$CuFeS_2$
CIS-WA-1	0.45/0.1620	30 cc	15 cc	15 cc	(1:1:0:0)	70°C	(103)	918	(W+CH)-$CuInS_2$
CIS-WA-6	0/0.5815	0 cc	55 cc	10 cc	(1:1:0:0)	140°C	(112)	750	CH-$CuInS_2$
CIS-WA-1	0.45/0.1620	30 cc	15 cc	15 cc	(1:1:0:0)	70°C	(103)	918	(W+CH)-$CuInS_2$
CIS-WA-2	0.45/0.1610	30 cc	15 cc	7.5 cc	(1:1:0:0)	70°C	(103)	1082	(W+CH)-$CuInS_2$
CIS-WA-3	0.45/0.1630	30 cc	15 cc	22.5 cc	(1:1:0:0)	70°C	(103)	784	(W+CH)-$CuInS_2$
CIS-WA-4	0.67/0.1600	45 cc	15 cc	0 cc	(1:1:0:0)	70°C	(103)	1024	(W+CH)-$CuInS_2$
CIS-WA-5	0.88/0.0	60 cc	0 cc	0 cc	(1:1:0:0)	70°C	(103)	1156	(W+CH)-$CuInS_2$
CIS-WA-6	0/0.5815	0 cc	55 cc	10 cc	(1:1:0:0)	140°C	(112)	750	CH-$CuInS_2$
CIS-WA-7	0/0.4728	0 cc	45 cc	20 cc	(1:1:0:0)	140°C	(112)	975	CH-$CuInS_2$
CIS-WA-8	0/0.3740	0 cc	35 cc	30 cc	(1:1:0:0)	140°C	(112)	990	CH-$CuInS_2$
CIS-WA-9	0/0.6500	0 cc	65 cc	0 cc	(1:1:0:0)	140°C	(112)	1000	CH-$CuInS_2$

[a]EDA: Ethylne diamine, [b]DEG: Diethylene glycol, [c]PEG: Polyethylene glycol, [d]CH: Chalcopyrite, [e]W: Wurtzite

sample number. The structures and optical properties of the $CuMS_2$ NCs were characterized using an X-ray diffraction spectrometer (Panalytical MPD), a transmission electron microscope (TEM, Hitachi S-4800), a UV–Vis-NIR spectrophotometer (Ocean Optics In. USB-4000) and photoluminescence (Fluoromax).

3. Results and discussion

The Al^{3+} is a one of the strongest Lewis acids, and the reduction potential of Al^{3+} is highly negative compared to Fe^{3+}, In^{3+} and Cu^{+}. As a result, the aluminum salt dissolves and reduces really hard in reaction, in comparison to copper, iron and indium precursors. For proper solving and reducing of aluminum salts, the oxidation/reduction reaction of $AlCl_3$ needs a strong reducer solvent, such as NH_4OH. The high chemical potential gap of the two half reactive species, and the high pressure and high temperature of the media provide energy to overcome a prohibitive activation energy barrier. Also, the amount of reducer is very important because the standard reduction potential for Al^{3+} is highly negative compared to NH_4OH, and adequate amounts of ammonium hydroxide are needed to reduce the aluminum ions (Eq. (1)):

$$E^0_{2NH_4OH\rightarrow N_2+H_2O+6H^+} = -0.092 \text{ V},$$

$$E^0_{Cu^+\rightarrow Cu} = +0.5180 \text{ V},$$

$$E^0_{Al^{3+}\rightarrow Al} = -1.660 \text{ V},$$

$$E^0_{In^{3+}\rightarrow In} = -0.3382 \text{ V},$$

$$E^0_{Fe^{3+}\rightarrow Fe} = -0.037 \text{ V},$$

$$E^0 = E^0_{\text{reduction}} - E^0_{\text{oxidation}} \prec 0. \quad (1)$$

Recent research [2-10,27-29] explains the formation mechanism of the complex for copper, aluminum, indium and iron, as below. If the precursors react with the amine functional group to form the complex, the mechanism of the reaction can be described as follows:

$$In_2(SO_4)_3 + 3/2C_2H_4(NH_2)_2 \rightarrow [In(EDA)_3]^{3+}, \quad (2)$$

$$AlCl_3 + 3/2C_2H_4(NH_2)_2 \rightarrow [Al(EDA)_3]^{3+}, \quad (3)$$

$$FeCl_3 + 3/2C_2H_4(NH_2)_2 \rightarrow\rightarrow [Fe(EDA)_3]^{3+}, \quad (4)$$

$$CuCl + 3/2C_2H_4(NH_2)_2 \rightarrow [Cu(EDA)]^{1+}. \quad (5)$$

If the metal salts react with the hydroxyl functional group to form the complex, the mechanism of the reaction can be described as follows:

$$In_2(SO_4)_3 + 3(HOCH_2CH_2)_2O \rightarrow [In(DEG)_3]^{3+}, \quad (6)$$

$$AlCl_3 + 3(HOCH_2CH_2)_2O \rightarrow [Al(DEG)_3]^{3+}, \quad (7)$$

$$FeCl_3 + 3(HOCH_2CH_2)_2O \rightarrow\rightarrow [Fe(DEG)_3]^{3+}, \quad (8)$$

$$CuCl + 3(HOCH_2CH_2)_2O \rightarrow [Cu(DEG)]^{1+}. \quad (9)$$

Also, the extra DEG, PEG and EDA can be used as a capping agent with the surface of the nanocrystal, which protects it from the agglomeration particles. At solution 2, thiourea and NH_4OH are used as sulfur ions and reducing agent, respectively:

$$4SC(NH_2)_2 + 3(HOCH_2CH_2)_2O + 8NH_4OH \rightarrow 4S^{2-}8H^+ + 16NH_3 + 4CO_2 + 3(HOCH_2CH_2)_2O. \quad (10)$$

When the anions solution (sulfur included) was injected into solution 1 (metal cations), fast nucleation was followed by the slow growth of the nanocrystal:

$$Cu^{1+} + Al^{3+} + 2S^{2-} \rightarrow CuAlS_2 + \text{by products}. \quad (11)$$

After forming the nanocrystal, the high temperature along with high pressure, in the autoclave, caused it to reach a good crystallinity phase.

The extra DEG, PEG, EDA and thiourea played the role of capping agent by reacting to the nanoparticles surface (amine NH_2, hydroxyl OH and thiol SH ligands). The capping agent controlled agglomeration with steric repulsion between particles.

The results indicate that the crystal structure of $CuAlS_2$, $CuInS_2$ and $CuFeS_2$ compounds are affected by different functional groups. This effect of the solvent is investigated for these three compounds, as well as the synthesis of $CuInS_2$, with the various molar ratios of functional groups. Figures 1 and 2 represent the XRD patterns of NCs that were synthesized by the amine and hydroxyl based solvents. Since Al^{3+} is a hard Lewis acid, the chemical reaction system needs to be extremely strong, coordinating and reducing the solvent in the synthesis of $CuAlS_2$. Different functional groups in the solvent can be investigated on the $CuAlS_2$ structural formation. A close study of the X-ray diffraction in Figure 1 shows that the intensity of the CAS-WA-19 sample is more than CAS-WA-14. It seems that the hydroxyl group can dissolve and reduce better in comparison with the amine based solvent. The structure of the synthesized $CuAlS_2$ is chalcopyrite, which matches well with the JCPDS 25-0014 card (Joint Committee of Powder Diffraction Standard). The main peaks for CAS-WA-14 are located in 29.370, 46.845, 58.090, and for CAS-WA-19 are

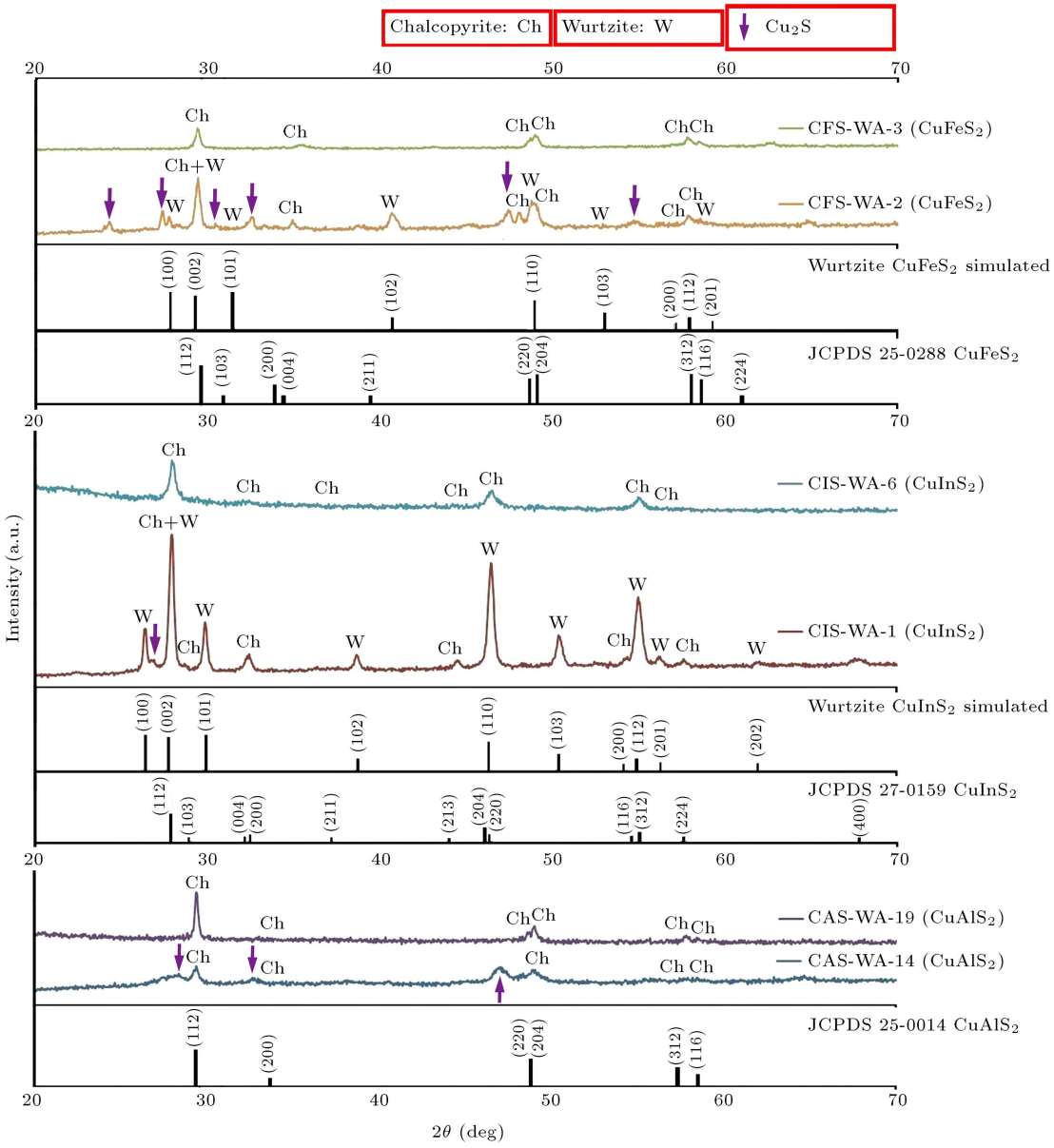

Figure 1. X-ray diffraction patterns of $CuAlS_2$, $CuFeS_2$ and $CuInS_2$ samples synthesized in the same conditions.

located in 29.331, 46.795, 57.803, which are assigned to (112), (204), (312) reflections of chalcopyrite $CuAlS_2$, respectively.

In contrast, the structure formation in the $CuInS_2$ compound is different to $CuAlS_2$. In the amine based solvent, the wurtzite structure forms beside the chalcopyrite structure. In fact, there is a polytypism in the $CuInS_2$ nanocrystalline, while, in the glycol based solvent, just the chalcopyrite structure exists. The main peaks of the wurtzite structure for the CIS-WA-1 sample are located in 26.3201, 27.8732, 29.8115, 38.6071 and 46.4041, which are assigned to (100), (002), (101), (102) and (110). Also, the chalcopyrite structure, along with the wurtzite structure, is also deduced from the XRD pattern of this sample (depicted in Figure 1). The (002) and (110) reflections of the wurtzite overlap to (112) and (204) reflections of chalcopyrite. For the glycol based solvent, the main peaks of the chalcopyrite structure for the CIS-WA-6 sample are located in 27.8919, 33.4151, 46.484 and 54.9632, which are assigned to (112), (200), (204) and (312). There is no wurtzite structure in this sample. The evolution of the XRD pattern (Figure 1) reveals that polytypism exists in the CFS-WA-2 sample (amine based solvent). Major diffraction peaks for $CuFeS_2$ (NCs) are observed at 2θ values of 27.300, 29.355, 32.520, 40.560 and 54.740, which are assigned to (100), (002), (101), (102) and (103). Also, the (002), (110) and (112) reflections of wurtzite are overlapped to (112), (204) and (312) reflections of chalcopyrite. For the glycol based solvent, the main peaks of the chalcopyrite structure for the CFS-

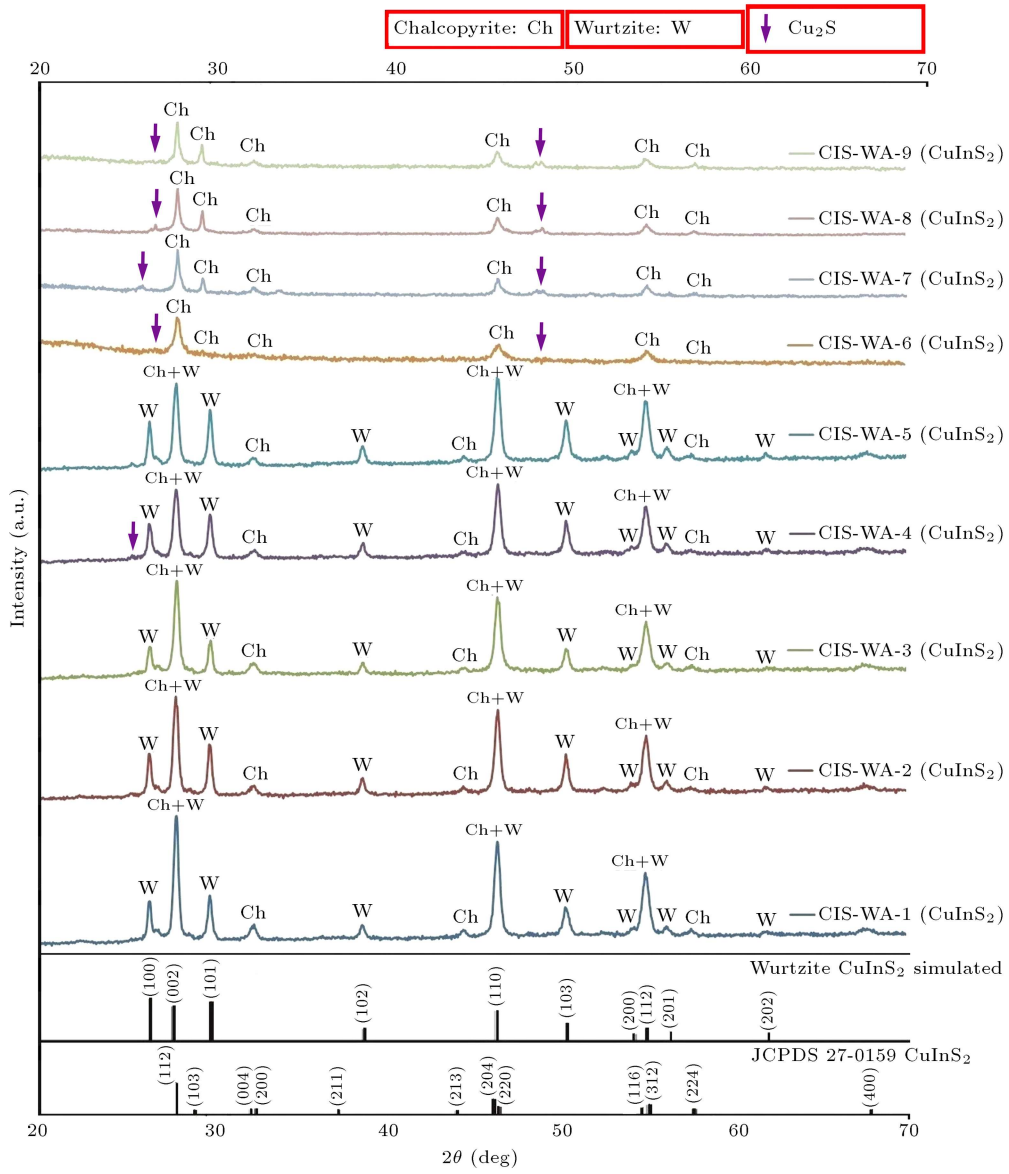

Figure 2. X-ray diffraction patterns of $CuInS_2$ samples synthesized in different ratios of functional groups.

WA-3 sample are located in 29.355, 35.375, 48.920, and 57.775 and 62.685 are assigned to (112), (200), (204), (312) and (224). In previous research, Kumar and coworkers [30] and Korgel and coworkers [31] investigated the polytypism of synthesized $CuInS_2$ and $CuFeS_2$ NCs.

Figure 2 shows the XRD patterns of synthesized $CuInS_2$ NCs of different functional group concentrations (ratio of amine to hydroxyl) that are effective in chalcopyrite or wurtzite structure formation. To investigate the formation mechanism of the wurtzite CIS NCs, the concentration ratio of NH_2 to OH was carried out, which can be expressed as follows: CIS-5>CIS-4>CIS-2>CIS-1>CIS-3. It can be seen that the intensity of wurtzite reflections is enhanced by increasing NH_2 concentration. Contrariwise, when the hydroxyl concentration increases, the chalcopyrite reflections enhance (as proof, increasing the intensity of the (103) reflection of wurtzite to the intensity of the (200) reflection of chalcopyrite). The intensity of the wurtzite main peaks can approximately demonstrate the amount of wurtzite structure formation. The (100), (101), (102) and (103) reflections are just for the wurtzite structure.

Table 1 confirms the (103) reflection for the wurtzite structure that is the maximum and the minimum for the CIS-WA-5 and CIS-WA-3, respectively, among the synthesized samples.

The lattice constants of the chalcopyrite and wurtzite structure (Scheme 1) of synthesized NCs can be calculated using the following formula [32]:

$$\frac{1}{d^2} = \frac{4}{3}\left(\frac{h^2+hk+k^2}{a^2}\right) + \frac{l^2}{c^2} \qquad \text{(Wurtzite)}, \quad (12)$$

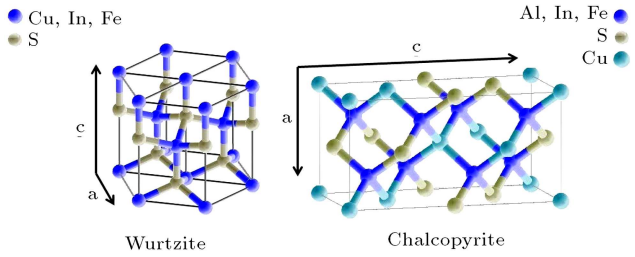

Scheme 1. The unit cells of wurtzite and chalcopyrite structures.

$$\frac{1}{d^2} = \frac{h^2 + k^2}{a^2} + \frac{l^2}{c^2} \qquad \text{(Chalcopyrite)}. \tag{13}$$

For the second batch of $CuInS_2$ samples, by synthesis with a glycol based solvent, the chalcopyrite structure is major. In these samples, the main peaks are just (112), (211), (204) and (312), and there are no main peaks for the wurtzite structure. Also, the crystallinity is enhanced by the increased amount of the hydroxyl functional group (Table 1). In fact, the types of functional groups in the reaction system are really effective on the formation of a major structure such as CIS-WA-9. On the other hand, the functional group properties of organic solvents are crucial to form a type of crystal structure. Both chalcopyrite and wurtzite structures are formed (polytypism) if there are both amine and hydroxyl in the reaction system (CIS-WA-1 to 5). It seems that the differences in strength of coordination and interaction of the solvent with the cations are critical to forming the crystal structure. The coordinating strength between EDA and DEG to metal ions is different to the formation of complexes. Besides, the low boiling point of EDA compared to DEG is really important. For EDA, the boiling point is 116°C. So, the reaction should proceed vigorously and the mixture may even be under a supercritical condition. The reaction conditions with DEG (high boiling point of 246°C) are quite different in these solvents, leading to the formation of different crystal phases [33-36]. It is interesting to see how mixtures of these solvents affect the produced crystal structures. By increasing contents of EDA from 30 cc to 60 cc, the wurtzite phase gradually increases.

Figure 3 shows typical TEM images obtained for three chalcopyrite compounds of $CuAlS_2$, $CuInS_2$ and $CuFeS_2$ samples, which are synthesized under the same conditions. As shown in Figure 3(a)-(f), the morphology of the particles seems cloud-like, which are attached to each other. It means that the cloud-like particles consist of aggregates of many nanoparticles with different sizes or morphology, or, probably, a different compound (lateral phase), which are loosely bound or interconnected with each other. In order to understand the growth mechanism of the $CuMS_2$ (M=Al, In and Fe) nanoparticles via the solvothermal method, on the basis of the obtained results, the aggregation morphology can be observed from Figure 3(a)-(f). The TEM images of samples $CuAlS_2$, $CuInS_2$ and $CuFeS_2$ are shown in Figure 3((a) and (d)), ((b) and (e)), ((c) and (f)), respectively. The average nanoparticle size of the aggregation products ranges from around 5-10 nm for $CuAlS_2$, 10-15 nm for $CuFeS_2$ to 20-50 nm for $CuInS_2$. This aggregation of nanoparticles in the solvothermal method can be obtained by high pressure in an autoclave, polymerization of the capping agent or solvent, an inappropriate capping agent (the length of hydrocarbon chains or natural capping agent), cross-linking molecules with two end groups and inadequate capping agents [37-48].

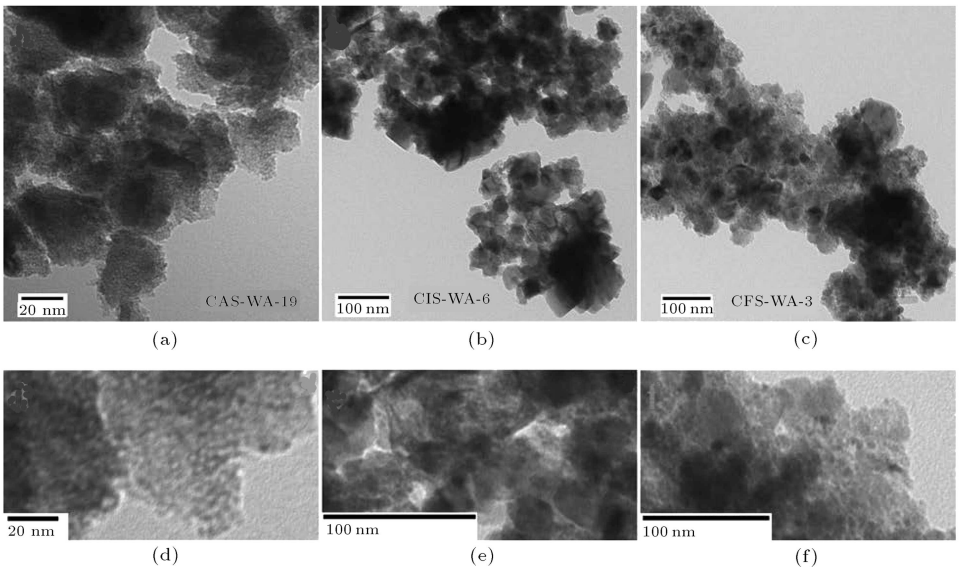

Figure 3. Representative TEM images of $CuAlS_2$ ((a) and (d)), $CuInS_2$ ((b) and (e)) and $CuFeS_2$ ((c) and (f)) nanoparticles.

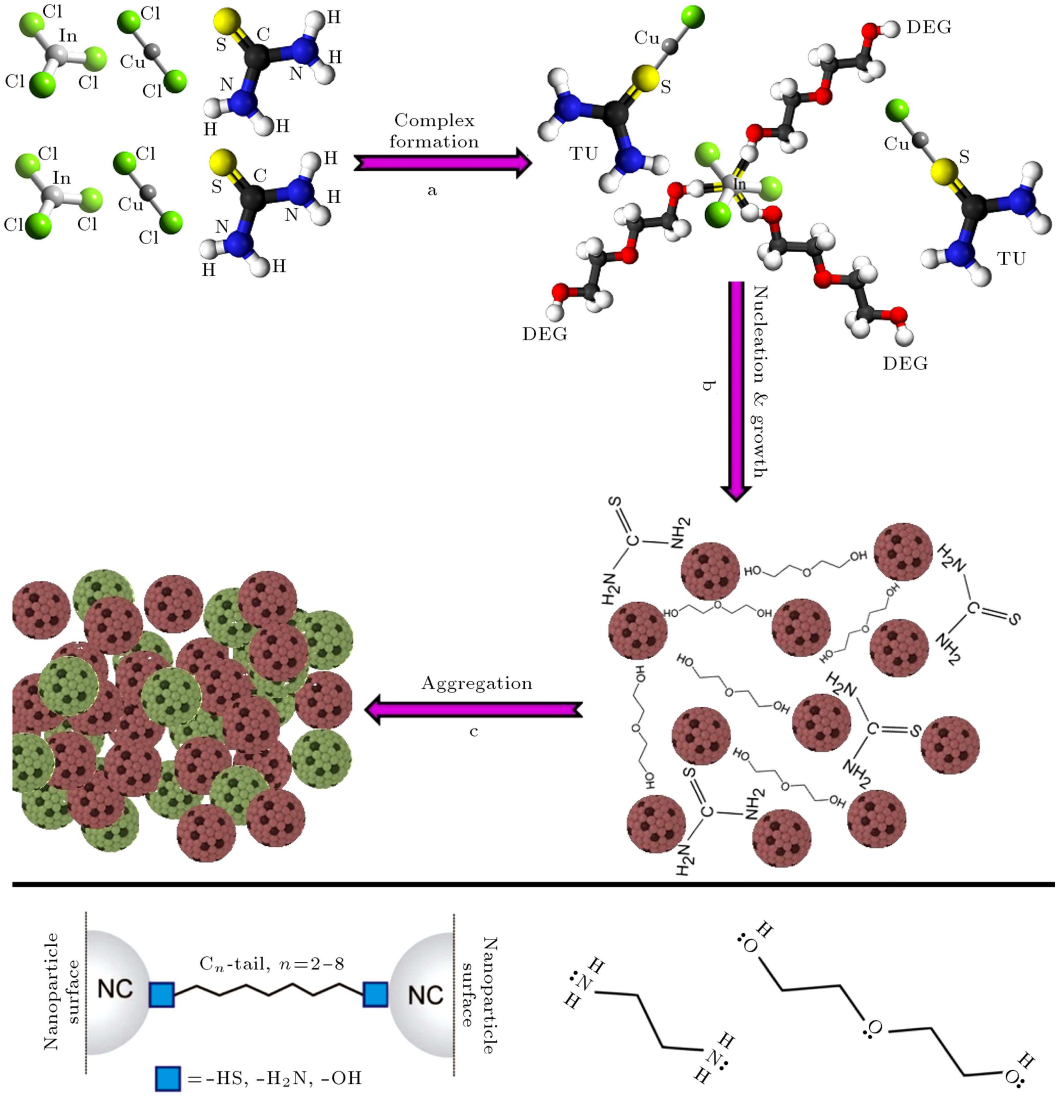

Scheme 2. The possible mechanism for synthesis of nanoparticles in autoclave.

A relative discussion of the aggregation model shown in Scheme 2 is suggested. In our reaction system, it seems that the aggregation has been resulted from the polymerization of the capping agent at a high pressure of the autoclave, and the small hydrocarbon chain length of glycols in comparison with the primary amine of the alkene (such as oleylamine).

The optical properties of $CuMS_2$ (M=Al, In and Fe) compound dispersed in Ethanol are measured at room temperature with UV-Vis absorption and PL spectra. The derived data from the pictures (Figures 4-7) shows that the edge of the absorption spectrum is around 356 nm for CAS-WA-19, 820 nm for CIS-WA-6 and 1880 nm for CFS-WA-3. Two absorption edges at 486 nm and 693 nm for $CuAlS_2$ (CAS-WA-19) are lateral phase ($Cu_{2-x}S$, $x = 0 - 1$). The optical band gaps for chalcopyrite NCs can be calculated from extrapolation of the linear portion of the $(\alpha h\nu)^2$ plots versus $h\nu$ to $\alpha = 0$. According to Figures 4-6, the absorption spectrum of the $CuAlS_2$, $CuInS_2$ and $CuFeS_2$ synthesized NCs show that all the samples have high absorption in the ultraviolet, visible and infrared regions, respectively. The band gap can be calculated to be 1.53 eV, 3.54 eV and 0.65 eV for CAS-WA-19, CIS-WA-6 and CFS-WA-3, respectively, with regard to the function of the photon energy $h\nu$ (a=absorption coefficient, h=Plank's constant and ν=frequency). Figure 7 shows the room temperature photoluminescence (PL) spectra of $CuAlS_2$ and $CuInS_2$ synthesized NCs dispersed in ethanol. A strong emission centered at 383 nm and 822 nm is observed in the photoluminescence (PL) spectrum upon exciting the sample at $\lambda = 260$ nm and $\lambda = 790$, respectively. The observed emission band can be assigned to the emission from the recombination of electrons and holes being conducted to the valence band. Besides, the weak emission peak can be assigned to trap surface states located in the Donor-

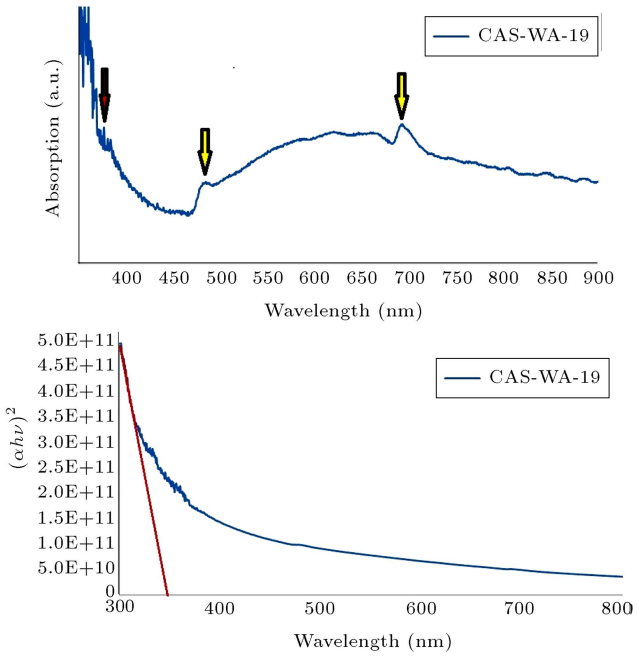

Figure 4. Optical absorption spectrum and band gap of CAS-WA-19 sample dispersed in ethanol.

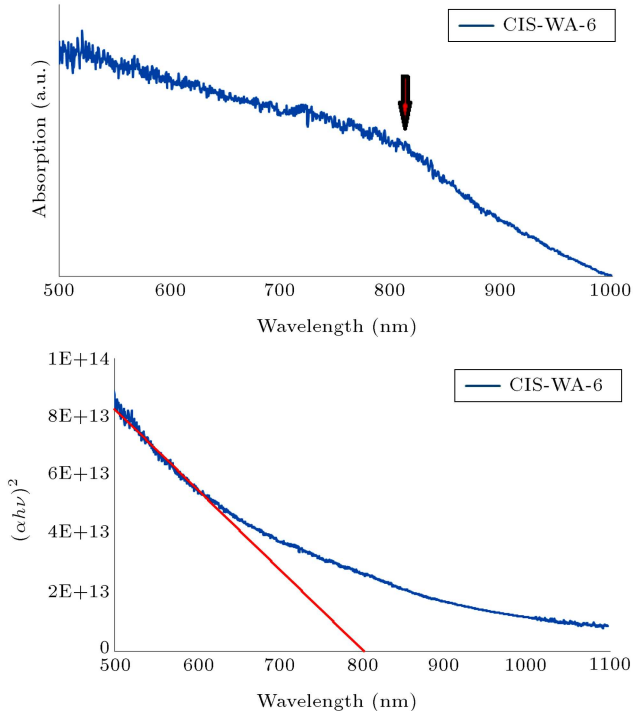

Figure 5. Optical absorption spectrum and band gap of CIS-WA-6 sample dispersed in ethanol.

Acceptor (DA) region of the band-gap (due to intrinsic defect).

4. Conclusion

In conclusion, a solvothermal approach has been developed for enhancing $CuAlS_2$ formation or for controlling

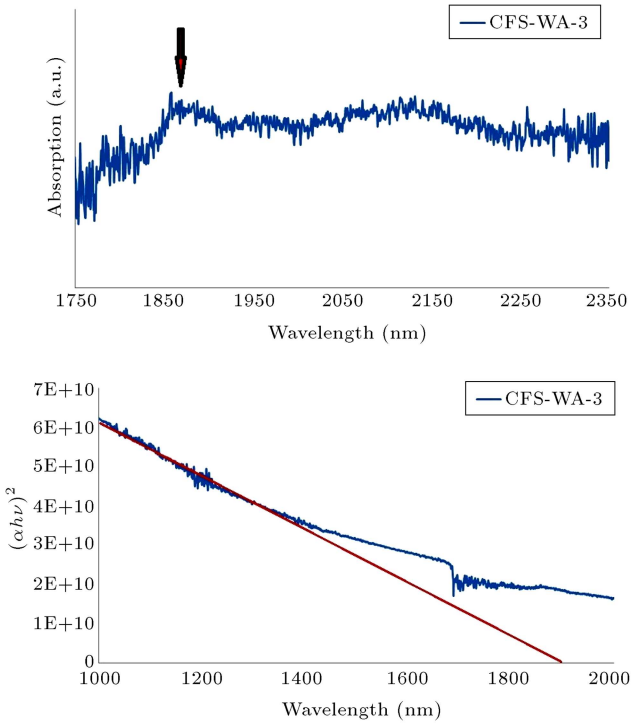

Figure 6. Optical absorption spectrum and band gap of CFS-WA-3 sample dispersed in ethanol.

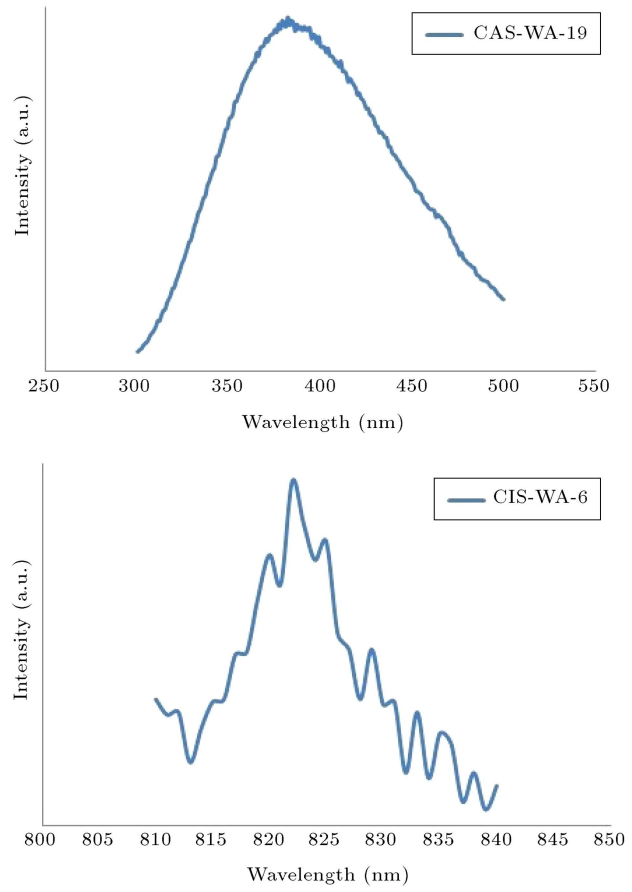

Figure 7. Photoluminescence spectrum of CAS-WA-19 and CIS-WA-6 sample dispersed in ethanol.

chalcopyrite and wurtzite formation in ternary $CuInS_2$ and $CuFeS_2$ compounds. For all these products, a pure chalcopyrite structure can be synthesized if strong coordinating solvents such as DEG are used, while the wurtzite phase, besides the chalcopyrite of these compounds, is favorable when using weaker coordinating solvents. It was also found that more wurtzite structures form when the amine group is used more than the hydroxyl group. By following the characterization of the optical, we find that high absorption occurs in the wavelength of the ultraviolet, visible and near infrared regions, respectively, for $CuAlS_2$, $CuInS_2$ and $CuFeS_2$ NCs.

References

1. Poulose, A.C., Veeranarayanan, S., Aravind, A., Nagaoka, Y., Yoshida, Y., Maekawa, T. and Kumar, D.S. "Synthesis of $CuAlS_2$ nanocrystals and their application in bio-imaging", *Mater. Express*, **2**(2), pp. 94-104 (2012).
2. Harichandran, G. and Lalla, N.P. "Facile synthesis of $CuAlS_2$ nanorods", *Mater. Lett.*, **62**(8-9), pp. 1267-1269 (2008).
3. Caglar, M., Ilican, S. and Caglar, Y. "Structural, morphological and optical properties of $CuAlS_2$ films deposited by spray pyrolysis method", *Opt. Commun.*, **281**(6), pp. 1615-1624 (2008).
4. Yue, G.H., Wang, X., Wang, L.S., Wang, W. and Peng, D.L. "Synthesis of single crystal $CuAlS_2$ nanowires via a low temperature direct polyol route", *Phys. Lett. A*, **372**(38), pp. 5995-5998 (2008).
5. Wang, Y.H.A., Bao, N. and Gupta, A. "Shape-controlled synthesis of semiconducting $CuFeS_2$ nanocrystals", *Solid State Sci.*, **12**(3), pp. 387-390 (2010).
6. Chen, G., Wang, L., Sheng, X., Liu, H., Pi, X. and Yang, D. "Chemical synthesis of Cu(In) metal inks to prepare $CuInS_2$ thin films and solar cells", *J. Alloys Compd.*, **507**(1), pp. 317-321 (2010).
7. Chen, G., Wang, L., Sheng, X. and Yang, D. "Direct synthesis of indium nanoparticles and their application to prepare $CuInS_2$ thin films and solar cells", *J. Sol-Gel Sci. Technol.*, **58**(1), pp. 162-169 (2011).
8. Luo, P., Yu, P., Zuo, R., Jin, J., Ding, Y., Song, J. and Chen, Y. "The preparation of $CuInSe_2$ films by solvothermal route and non-vacuum spin-coating process", *Phys. B*, **405**(16), pp. 3294-3298 (2010).
9. Park, M.S., Han, S.Y., Lee, E.J., Chang, C.H. and Ryu, S.O. "Synthesis and characterization of polycrystalline $CuInS_2$ thin films for solar cell devices at low temperature processing conditions", *Curr. Appl. Phys.*, **10**(3), pp. S379-S382 (2010).
10. Wei, H., Guo, W., Sun, Y., Yang, Z. and Zhang, Y. "Hot-injection synthesis and characterization of quaternary $Cu_2ZnSnSe_4$ nanocrystals", *Mater. Lett.*, **64**(13), pp. 1424-1426 (2010).
11. Yousefi, M., Sabet, M., Salavati-Niasari, M. and Hosseinpour-Mashkani, S.M. "Microwave approach for synthesis of copper-indium sulfide nanoparticles and study of their behavior in solar cell", *J. Clust. Sci.*, **23**(2), pp. 491-502 (2012).
12. Pop, A.E., Popescu, V., Danila, M. and Batin, M.N. "Optical properties of Cu_xS nanopowders", *Chalcogenide Lett.*, **8**(6), pp. 363- 370 (2011).
13. Cushing, B.L., Kolesnichenko, V.L. and O'Connor, C.J. "Recent advances in the liquid-phase syntheses of inorganic nanoparticles", *Chem. Rev.*, **104**(9), pp. 3893-3946 (2004).
14. Vahidshad, Y., Tahir, M.N., Iraji-Zad, A., Mirkazemi, S.M., Ghasemzadeh, R., Huesmann, H. and Tremel, W. "Structural and optical study of Ga^{3+} substitution in $CuInS_2$ nanoparticles synthesized by a one-pot facile method", *J. Phys. Chem. C*, **118**(42), pp. 24670-24679 (2014).
15. Long, F., Wang, W.M., Tao, H.C., Jia, T.K., Li, X.M., Zou, Z.G. and Fu, Z.Y. "Solvothermal synthesis, nanocrystal print and photoelectrochemical properties of $CuInS_2$ thin film", *Mater. Lett.*, **64**(2), pp. 195-198 (2010).
16. Wei, Q. and Mu, J. "Synthesis of $CuInS_2$ nanocubes by a wet chemical process", *J. Dispersion Sci. Technol.*, **26**(5), pp. 555-558 (2005).
17. Kuzuya, T., Hamanaka, Y., Itoh, K., Kino, T., Sumiyama, K., Fukunaka, Y. and Hirai, S. "Phase control and its mechanism of $CuInS_2$ nanoparticles", *J. Colloid Interface Sci.*, **388**(1), pp. 137-143 (2012).
18. Dutta, D.P. and Sharma, G. "A facile route to the synthesis of $CuInS_2$ nanoparticles", *Mater. Lett.*, **60**(19), pp. 2395-2398 (2006).
19. Sabet, M., Salavati-Niasari, M., Ashjari, M., Ghanbari, D. and Dadkhah, M. "$CuInS_2$/CuS nanocomposite: Synthesis via simple microwave approach and investigation its behavior in solar cell", *J. Inorg. Organomet. Polym. Mater.*, **22**(5), pp. 1139-1145 (2012).
20. Sheng, X., Wang, L. and Yang, D. "Shape and size controlled synthesis of $CuInS_2$ particles in polyalcohol system used as "printable ink" for thin films", *J. Sol-Gel Sci. Technol.*, **62**(1), pp. 87-91 (2012).
21. Mousavi-Kamazani, M., Salavati-Niasari, M. and Ghanbari, D. "A facile solvothermal method for synthesis of $CuInS_2$ nanostructures", *J. Nanostruct.*, **2**(3), pp. 363-368 (2012).
22. Steinhagen, C., Panthani, M.G., Akhavan, V., Goodfellow, B., Koo, B. and Korgel, B.A. "Synthesis of Cu_2ZnSnS_4 nanocrystals for use in low-cost photovoltaics", *J. Am. Chem. Soc.*, **131**(35), pp. 12554-12555 (2009).

23. Pei, L.Z., Wang, J.F., Tao, X.X., Wang, S.B., Dong, Y.P., Fan, C.G. and Zhang, Q.F. "Synthesis of CuS and $Cu_{1.1}Fe_{1.1}S_2$ crystals and their electrochemical properties", *Mater. Charact.*, **62**(3), pp. 354-359 (2011).

24. Aldakov, D., Lefrançois, A. and Reiss, P. "Ternary and quaternary metal chalcogenide nanocrystals: Synthesis, properties and applications", *J. Mater. Chem. C*, **1**(24), pp. 3756-3776 (2013).

25. Vahidshad, Y., Ghasemzadeh, R., Irajizad, A., Mirkazemi, M. and Masoud, A. "Synthesis and characterization of $CuAlS_2$ nanoparticles by facile heat arrested method", *J. Nanostruct.*, **2**(3), pp. 369-377 (2012).

26. Vahidshad, Y., Irajizad, A., Ghasemzadeh, R., Mirkazemi, M. and Masoud, A. "Structural and optical characterization of nanocrystalline $CuAlS_2$ chalcopyrite synthesized by polyol method in autoclave", *Int. J. Mod. Phys. B*, **26**(31), pp. 1250179-1250191 (2012).

27. Vahidshad, Y., Ghasemzadeh, R., Irajizad, A. and Mirkazemi, M. "Synthesis and characterization of copper indium sulfide chalcopyrite structure with hot injection method", *J. Nanostruct.*, **3**(2), pp. 145-154 (2013).

28. Alwan, T.J. and Jabbar, M.A. "Structure and optical properties of $CuAlS_2$ thin films prepared via chemical bath deposition", *Turk. J. Phys.*, **34**(2), pp. 107-116 (2010).

29. Permadi, A., Fahmi, M.Z., Chen, J.K., Chang, J.Y., Cheng, C.Y., Wang, G.Q. and Ou, K.L. "Preparation of poly(ethylene glycol) methacrylate coated $CuInS_2$/ZnS quantum dots and their use in cell staining", *RSC Adv.*, **2**(14), pp. 6018-6022 (2012).

30. Kumar, P., Uma, S. and Nagarajan, R. "Precursor driven one pot synthesis of wurtzite and chalcopyrite $CuFeS_2$", *R. Chem. Commun.*, **49**(66), pp. 7316-7318 (2013).

31. Koo, B., Patel, R.N. and Korgel, B.A. "Wurtzite-chalcopyrite polytypism in $CuInS_2$ nanodisks", *Chem. Mater.*, **21**(9), pp. 1962-1966 (2009).

32. Cullity, B.D., *Elements of X-ray Diffraction*, pp. 95-135, Addision-Wesley Publishing Company Inc., London, UK (1978).

33. Huang, W.C., Tseng, C.H., Chang, S.H., Tuan, H.Y., Chiang, C.C., Lyu, L.M. and Huang, M.H. "Solvothermal synthesis of zincblende and wurtzite $CuInS_2$ nanocrystals and their photovoltaic application", *Langmuir*, **28**(22), pp. 8496-8501 (2012).

34. Li, Y., Han, Q., Kimb, T.W. and Shi, W. "Synthesis of wurtzite-zincblende Cu_2ZnSnS_4 and $Cu_2ZnSnSe_4$ nanocrystals: Insight into the structural selection of quaternary and ternary compounds influenced by binary nuclei", *Nanoscale*, **6**(7), pp. 3777-3785 (2014).

35. Qi, Y., Liu, Q., Tang, K., Liang, Z., Ren, Z. and Liu, X. "Synthesis and characterization of nanostructured wurtzite $CuInS_2$: A new cation disordered polymorph of $CuInS_2$", *J. Phys. Chem. C*, **113**(10), pp. 3939-3944 (2009).

36. Bao, N., Qiu, X.H.Y., Wang, A., Zhou, Z., Lu, X., Grimes, C.A. and Gupta, A. "Facile thermolysis synthesis of $CuInS_2$ nanocrystals with tunable anisotropic shape and structure", *Chem. Commun.*, **47**(33), pp. 9441-9443 (2011).

37. Ålander, E.M., Penttila, M.S.U. and Rasmuson, Å.C. "Agglomeration of paracetamol during crystallization in pure and mixed solvents", *Ind. Eng. Chem. Res.*, **43**(2), pp. 629-637 (2004).

38. Talapin, D.V., Lee, J.-S., Kovalenko, M.V. and Shevchenko, E.V. "Prospects of colloidal nanocrystals for electronic and optoelectronic applications", *Chem. Rev.*, **110**(1), pp. 389-458 (2010).

39. Zhou, Y., Zhou, W., Li, M., Du, Y. and Wu, S. "Hierarchical Cu_2ZnSnS_4 particles for a low-cost solar cell: Morphology control and growth mechanism", *J. Phys. Chem. C*, **115**(40), pp. 19632-19639 (2011).

40. Zhou, Y.L., Zhou, W.H., Du, Y.F., Li, M. and Wu, S.X. "Sphere-like kesterite Cu_2ZnSnS_4 nanoparticles synthesized by a facile solvothermal method", *Mater. Lett.*, **65**(11), pp. 1535-1537 (2011).

41. Zaberca, O., Gillorin, A., Durand, B. and Ching, J.Y.C. "A general route to the synthesis of surfactant-free, solvent-dispersible ternary and quaternary chalcogenide nanocrystals", *J. Mater. Chem.*, **21**(18), pp. 6483-6486 (2011).

42. Gong, M., Kirkeminde, A. and Ren, S. "Symmetry-defying iron pyrite (FeS_2) nanocrystals through oriented attachment", *Sci. Rep.*, **3**(2092), pp. 1-6 (2013).

43. He, L., Wang, M., Ge, J. and Yin, Y. "Magnetic assembly route to colloidal responsive photonic nanostructures", *Acc. Chem. Res.*, **45**(9), pp. 1431-1440 (2012).

44. Abargues, R., Albert, S., Vald, J.L., Abderrafi, K. and Martinez-Pastor, J.P. "Molecular-mediated assembly of silver nanoparticles with controlled interparticle spacing and chain length", *J. Mater. Chem.*, **22**(41), pp. 22204-22211 (2012).

45. Dang, C., Lee, J., Breen, C., Steckel, J.S., Coe-Sullivan, S. and Nurmikko, A. "Red, green and blue lasing enabled by single-exciton gain in colloidal quantum dot films", *Nat. Nanotechnol.*, **7**(5), pp. 335-339 (2012).

46. Ip, A.H., Thon, S.M., Hoogland, S., Voznyy, O., Zhitomirsky, D., Debnath, R., Levina, L., Rollny, L.R., Carey, G.H., Fischer, A., Kemp, K.W., Kramer, I.J., Ning, Z., Labelle, A.J., Chou, K.W., Amassian, A. and Sargent, E.H. "Hybrid passivated colloidal quantum dot solids", *Nat. Nanotechnol.*, **7**(5), pp. 577-582 (2012).

47. Xia, Y. and Tang, Z. "Monodisperse inorganic supraparticles: Formation mechanism, properties and ap-

plications", *Chem. Commun.*, **48**(51), pp. 6320-6336 (2012).

48. Yang, P., Arfaoui, I., Cren, T., Goubet, N. and Pileni, M.P. "Unexpected electronic properties of micrometer-thick supracrystals of Au nanocrystals", *Nano Lett.*, **12**(4), pp. 2051-2055 (2012).

Biographies

Yaser Vahidshad was born in Kashan, Iran, in 1979, and received BS and MS degrees in Materials Science from Sahand University of Technology, Tabriz, Iran, in 2002 and the University of Tehran, Iran, in 2008, respectively. He is currently pursuing his PhD degree at Iran University of Science and Technology. His research interests include semiconducting material synthesis applicable in photovoltaic.

Reza Ghasemzadeh obtained his PhD degree from Imperial College, England, in 1973, and became a faculty member of Iran University of Science and Technology, in 1973. His research interests include extractive metallurgy, transport phenomena, fuels, energy, and furnaces.

Azam Iraji Zad obtained her PhD degree in Surface Physics from Sussex University, Brighton, UK, in 1990, and became a faculty member of Sharif University of Technology, Tehran, Iran, in 1990. Her research interests include thin films deposition and characterization, and electrical, magnetic and optical properties of thin films.

Seyed Mohammad Mirkazemi obtained his PhD degree in 2005 from Iran University of Science and Technology, Iran, where he is currently faculty member. His research interests include glass-ceramics, nanomaterials, magnetic materials, and advanced ceramic materials.

A. Masoud. His/her biography was not available at the time of publication.